Metal-Ceramic Composites Based on the Ti-B-Cu Porosity System

H.P. LI, S.B. BHADURI, and J.A. SEKHAR

A systematic study of the microstructure/fracture toughness/processing correlation of metal-ceramic composites in the Ti-B-Cu porosity system is presented. The composites are produced by the combustion synthesis process. Fracture surfaces indicate both ductile and brittle regions. The composites are made up of Ti as the only ductile phase and TiB, TiB_2, Ti_2Cu, and Ti_3Cu_4 as brittle phases. Density measurements and scanning electron microscopy (SEM) indicate that the samples contain distributed porosity. Ductile phase toughening is responsible for the increase in fracture toughness to a maximum value of 9.9 $MPa(m)^{1/2}$. Samples with large amounts of porosity do not benefit from this toughening process even though they contain *in situ* formed whiskers. The fracture toughness of the composite is modeled by considering the additive influence of the ductile phase reinforcement (Ashby model) and the residual porosity (exponential model). Microstructural constants required for the model are evaluated from the comparison. A correlation between the mechanical properties and the combustion temperature is established.

I. INTRODUCTION

CERAMIC materials have potential uses in challenging engineering application on account of being hard, refractory, and corrosion- and erosion-resistant. The primary drawback of many ceramic materials is their inherent brittleness. They are also prone to thermal shock and fast crack growth. Therefore, ceramics are often not reliable in critical engineering usages. The inherent brittleness is a problem in fabricating components. Most often, the fabrication is undertaken using powder technology.[1,2] As compared to ceramics, metals are tough but commonly cannot withstand high temperatures. It may therefore be expected that metal-ceramic composites will possess good hardness, toughness, strength, and may not be susceptible to undesirable fatigue, thermal shock, and environmental attack. The reinforcement in the composites may be discontinuous[3,4] or continuous.[5]

The goal of this article is to study the mechanical property, microstructure, and processing correlations in metal-ceramic composites made by the combustion synthesis route. Specifically, the study focuses on composites fabricated from a ternary system of Ti(titanium)-B(boron)-Cu(copper). The interest in this system originates from the fact that elemental powders of Ti and B, when processed by powder metallurgy (PM), react to form a ceramic material TiB_2 (the equilibrium binary phase diagram of Ti-B is shown in Figure 1[6]). The process allows for the direct fabrication of parts without a sintering step.[7-14] The advantage is that it is a simple process for producing high-temperature materials. The disadvantage is that, most often, the product is porous. Therefore, the product is crushed and sintered/hot pressed to achieve full density. One may, in principle, bypass this difficulty by incorporating a third metal, which would reduce the reactivity of the violent reaction and melt during the exothermic reaction and fill the pores.[7-14] By such an approach, the porosity may be reduced to lower than 3 pct[13] while simultaneously increasing the hardness significantly.[13] Additionally, the toughness may be increased by the incorporation of a ductile phase in a brittle ceramic.[15,16] In this article, Cu is tried as a candidate material. This article reports on the microstructure and fracture toughness of the metal-ceramic composite materials consisting of various ratios of Ti, B, and Cu produced by the combustion synthesis process.

Several studies have been reported on ductile phase reinforcement. Typical matrices used were NaCl, MgO, glass, Al_2O_3, and ZrO_2.[17-21] The reinforcements were typically refractory metals such as Mo and other metals such as Fe, Co, Ni, and Zr.[17-21] However, contrary to the expected high increase in the value of toughness, the toughness was seen to improve only marginally. Rankin *et al.*[22] reported an 80 pct increase in fracture surface energy by incorporating Mo in Al_2O_3. Similar increases were reported by Virkar and Johnson.[23] These increases are well below the toughness levels achieved in a transformation-toughened ZrO_2 system without using any metallic reinforcement. One notable piece of work is by Mendelson and Fine,[24] who reported a 160 pct increase in toughness by adding Fe to FeO matrix.

A common observation in these studies was the lack of deformation of particles during fracture on account of the ductile phase not being properly utilized. This is due to the fact that the second-phase/matrix interface surface energy was not optimized. This problem has been studied and remedied by several groups[25-30] on various combinations of matrices and particles.

To further elucidate the nature of deformation, Ashby

H.P. LI, Graduate Research Assistant, Department of Materials Science and Engineering, and J.A. SEKHAR, Associate Professor, Department of Materials Science and Engineering, and Director, Center for Micropyretics, are with the University of Cincinnati, Cincinnati, OH 45221-0012. S.B. BHADURI, formerly with the Department of Materials Science and Engineering, University of Cincinnati, is with the University of Idaho, Moscow, ID 83843.

Manuscript submitted April 11, 1991.

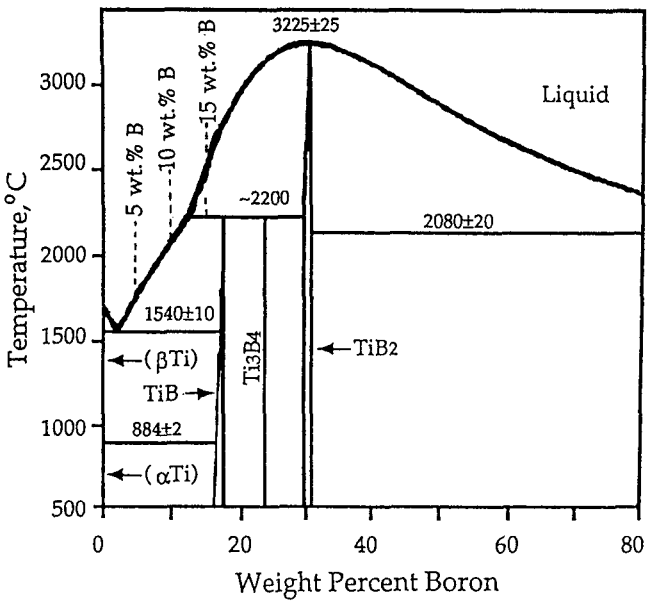

Fig. 1—Ti-B binary phase diagram[6] with chosen compositions for making the composites.

et al.[31] performed an elegant experiment. They introduced molten lead in a PYREX* glass capillary and studied the stress-strain behavior. The deformation behavior of such a wire was strongly influenced by its constrained state. Three types of failure mechanisms were observed: (a) internal void growth in the metal, (b) decohesion at the metal-matrix interface, and (c) cracking at the brittle matrix. Based on the above findings, a testing procedure for testing mechanical properties of TiAl-Nb composites was described by Cao *et al.*[32] A cylindrical specimen with a notch was deformed in uniaxial tension, and the stress-strain curve was plotted in the optical camera system. The toughness of brittle intermetallics could be calculated from the curve.

*PYREX is a trademark of Corning Glass Works, Corning, NY.

Several models of ductile phase toughening exist.[27–33] The model of Krstic *et al.*[27] predicts that the increase in toughness varies with square root of the particle size, linearly with the yield stress of the second phase, and inversely with $[1 + (2/3)((1/V_f) - 1)]^2$, where V_f is the volume fraction of second phase. The experimental data of glass-Ni composite of Krstic *et al.* match well with the predictions of the model. The drawback of several models, except that by Ashby *et al.*,[31] is that the constrained deformation of second-phase particles is not considered. This is so because it is inherently assumed that the second-phase particles are strongly bonded to the matrix. In cases where they are not tightly bonded to the matrix, they pull free from the matrix, and the concept of ductile toughening is defeated. The small-scale yielding approach used in the many models may not be totally valid during the straining of the ductile phase.

The aforementioned difficulties were understood by several authors. For example, Evans and McMeeking[34] analyzed the slip line method. They consider the initial interaction between the crack and the particle to be of small-scale yielding after which large-scale yielding ensues. The model proposed by Ashby *et al.*[31] assumes that the crack is attracted to particles or wires and does not bypass them. The increase fracture toughness due to the ductile phase can now be expressed as

$$\Delta K_{\text{reinforced}} = E\left[CV_f \frac{\sigma_0}{E} a_0\right]^{1/2} \quad [1]$$

where E is the Young's modulus of the inclusion, σ_0 is the yield strength of ductile phase, C is a constant, a_0 is the radius of the particle or wire, and V_f is the volume fraction of the ductile phase. The value of the constant C depends on complete bonding or limited debonding. From this expression, we note that the greatest toughening is obtained from inclusions with a high volume fraction V_f, modulus E, strength σ_0, and a large radius a_0. This is also the first model which lends itself to easy experimental verification.

The influence of porosity on fracture toughness has been examined by Kendall *et al.*,[35] Rice *et al.*,[36] and Mai and Cotterell.[37] They suggested that the fracture toughness data may be described by an exponential function in porosity:

$$K_{IC} = K_m \exp(-bp) \quad [2]$$

where p is porosity, K_m is the fracture toughness of the matrix without porosity, and b is a constant. The decrease in fracture toughness in the presence of porosity is because porosity aids the crack propagation. Experimental values[37] of a decrease in fracture toughness fit well with the equation given above.

II. EXPERIMENTAL PROCEDURE

Samples were obtained by mixing powders, pressing them into shape, and finally combusting the shape from one end and allowing heat from the combustion wave to densify the material. The particle sizes of titanium and amorphous boron powders were −325 mesh and that of copper powder was −100 mesh. Initially, three ratios of Ti and B were chosen, 95:5, 90:10, and 85:15 by weight. These are nonstoichiometric compositions. In order to reduce the reactivity of the combustion reaction and densify the compacts, these compositions were further mixed with 10 and 20 wt pct Cu. In effect, nine compositions were studied, as shown in Table I. In order to easily recognize each composition, a two-number symbol indication was used for different compositions. The first number indicates the ratio of B content in Ti-B and the

Table I. The Compositions Studied in this Work

Compositions	Ti:B	Wt Pct Cu	Ti : B :Cu
5-0	95:5	0 pct	95 : 5 0
5-10	95:5	10 pct	85.5: 4.5:10
5-20	95:5	20 pct	76 : 4 :20
10-0	90:10	0 pct	90 :10 : 0
10-10	90:10	10 pct	81 : 9 :10
10-20	90:10	20 pct	72 : 8 :20
15-0	85:15	0 pct	85 :15 : 0
15-10	85:15	10 pct	76.5:13.5:10
15-20	85:15	20 pct	68 :12 :20

latter, the Cu content, in the ternary system. For example, composition 10-20 means Ti:B = 90:10 and (Ti-B):Cu = 80:20 (*i.e.*, Ti:B:Cu = 72:8:20). The well-mixed powder was pressed at a pressure of 15,000 psi (~100 MPa), using a double-acting die to form an ASTM-E8M standard specimen. The sample thickness varied from 4.5 to 6.0 mm. The compacted specimen was then combustion synthesized by igniting from one end with an oxy-acetylene torch. The values of density and initial porosity were measured by the ASTM C373 standard.[38]

The samples were sectioned and coated with gold-palladium for scanning electron microscopy (SEM) observations with secondary electron imaging. These micrographs were further processed by scanning them using a digital scanner and analyzing for microstructural features. From the fractographs, the amounts and sizes of the phases and pores were measured by digitally scanning the fractographs in an image analysis system and acquiring statistically significant information from several fractographs. For some of the microstructures, energy-dispersive X-ray analysis (EDAX) was performed to obtain compositional data (except boron). X-ray diffraction work was carried out in a SIEMENS* diffractometer (model: Diffrac 11) and Ni-filtered Cu tube (wavelength: 0.154051 nm) operating at 40 KV and 30 mA. The scanning speed employed was 0.01 degree/s. The X-ray patterns of the pure materials were used as a reference. From these, *i.e.*, by calibrating the standard patterns, the relative weight percentages of the various phases were calculated by integrating the intensity area and relating the same to the weight percentage.

*SIEMENS is a trademark of The Retton & Crane Company, Cupertino, CA.

A very fine tungsten-rhenium (W-5 pct Re and W-26 pct Re) thermocouple was used to measure combustion temperature. The thermocouple was embedded in the center area of the sample, with a depth of half the sample height. A data acquisition system and MACINTOSH* computer recorded the input temperature at every 0.1-second interval.

*MACINTOSH is a trademark of Apple Computers, Inc., Cupertino, CA.

Edge-notched beam technique (NB) was used to determine the fracture toughness of materials. The material was assumed to be isotropic. The notch was introduced by low-speed thin diamond blade. The value of K_{IC} was calculated by the reported form of the Griffith relation.[39] A universal testing machine was used for monitoring the load.

III. RESULTS AND DISCUSSION

A. *Density and Porosity*

The theoretical density, green density, and final density values as well as porosity values are shown in Table II. The initial porosity values determine the state of compaction of the samples. For most of the samples, an initial green density of ~60 pct of the theoretical density is required for producing sound samples. It was observed that if the initial porosity level is high, the state of compaction is not satisfactory, resulting in poor handling strength. With low initial porosity, the exothermic reaction is not self-propagating. The final porosity values were obtained in the bulk samples from the analysis of the sectioned surfaces. From Table II we note that an increase in the B content increases porosity, whereas the porosity reduces on addition of Cu.

B. *X-Ray Diffraction and Phase Analysis*

The X-ray diffraction (XRD) patterns for the various compositions are identified from ASTM cards. The summary of the compositions of the reaction products is shown in Table III. It shows that in the case of samples without Cu, the major constituents are Ti and TiB. This is expected from the equilibrium binary phase diagram of Ti-B, as shown in Figure 1. The chosen compositions are close to TiB rather than TiB_2. Titanium boride forms rather than TiB_2, even though the enthalpy of formation at room temperature for TiB_2 (−66.8 Kcal/mole)[40] is higher than TiB (−38.3 Kcal/mole).[40] The rest of the material contains free Ti. With an increase in B in the composition, the amount of TiB increases and Ti goes down. With Ti:B in the ratio 85:15, the TiB is still a major peak, but the presence of Ti and some TiB_2 is also noted.

Addition of Cu to the Ti-B compositions brings about a dramatic change in the X-ray pattern. Intermetallic compounds in the Ti-Cu binary system (namely, Ti_2Cu

Table II. Density and Porosity of Green and Processed Samples*

Compositions	Theoretical Density	Green Density	Final Bulk Density	Initial Porosity	Final Porosity
5-0	4.31	2.64 ± 0.03	3.11 ± 0.10	38.8 ± 0.4	~32
5-10	4.51	2.78 ± 0.02	3.18 ± 0.08	38.4 ± 0.3	~10
5-20	4.73	3.06 ± 0.18	3.48 ± 0.09	35.3 ± 2.1	~14
10-0	4.13	2.46 ± 0.07	NA**	40.4 ± 1.2	~58
10-10	4.30	2.67 ± 0.05	3.07 ± 0.04	37.9 ± 0.7	~17
10-20	4.49	2.86 ± 0.01	3.12 ± 0.43	36.3 ± 0.1	~19
15-0	3.96	2.32 ± 0.08	NA**	41.4 ± 1.4	~53
15-10	4.11	2.47 ± 0.08	2.57 ± 0.03	39.9 ± 1.3	~33
15-20	4.27	2.53 ± 0.12	3.41 ± 1.47	40.8 ± 1.9	~45

*Units: density (g/cm^3); porosity (pct).
**These values are not available because the pores are too large in these samples.

Table III. Estimated Content of Phases (Weight Percent) in Reacted Compositions

Compositions	>50 Pct	40 ~ 50 Pct	30 ~ 40 Pct	20 ~ 30 Pct	10 ~ 20 Pct	<10 Pct
5-0	Ti	—	TiB	—	—	TiB_2
5-10	—	Ti	Ti_2Cu	—	TiB	TiB_2
5-20	—	—	Ti	Ti_3Cu_4	TiB, Ti_2Cu	TiB_2
10-0	—	Ti, TiB	—	—	—	TiB_2
10-10	—	—	Ti	TiB	Ti_2Cu, Ti_3Cu_4	TiB_2
10-20	—	—	—	TiB, Ti_3Cu_4	Ti, TiB_2, Ti_2Cu	—
15-0	—	—	TiB	TiB_2	Ti	—
15-10	TiB	—	—	—	TiB_2, Ti_3Cu_4	Ti
15-20	TiB	—	—	—	Ti_3Cu_4	Ti, TiB_2, Ti_2Cu

and Ti_3Cu_4) now dominate the X-ray pattern. While in the case of composition 5-10 (Ti:B:Cu = 85.5:4.5:10), both Ti_2Cu and free Ti are noted, the amount of Ti_3Cu_4 goes up in compositions 10-10 (Ti:B:Cu = 81:9:10) and 15-10 (Ti:B:Cu = 76.5:13.5:10). With further increase in Cu, the amount of Ti_3Cu_4 increases. The enthalpies of formation of these compounds are not available in the literature. However, the results are seen to follow the intermetallics that are expected from the binary phase diagram as the Cu content is increased.

C. *Micrography*

Figure 2 shows the scanning electron micrographs of the compositions with 10 wt pct Cu. As the boron content increases, the total volume of porosity, as well as the size of porosity, increases. However, with the incorporation of Cu, the pores are filled by molten Cu. A lowering in porosity is noted with increasing Cu, increasing again as the boron content increases (Table II).

Fractographs are taken from samples broken in the notched bend test. Figure 3 shows the fractographs of the Ti:B = 95:5 series compositions. Figure 3(a), 0 wt pct Cu composition, reveals a somewhat ductile fracture of the material. This is due to the presence of free Ti revealed by the XRD pattern. The 10 wt pct Cu composition (Figure 3(b)) shows more brittle fracture. Also noted is the transgranular fracture of large particles. It is interesting to note that in 20 wt pct Cu composition (Figure 3(c)), the ductile fracture occurs around the brittle phase; *i.e.*, there seems to be just enough Ti in the system to bind the brittle particle.

Compositions in the Ti:B = 90:10 series have similar features, as noted in the fractograph of the Ti:B = 95:5 series compositions. A new feature of the microstructure is shown in Figure 4, where it is shown that the pores contain whiskerlike objects. Energy-dispersive X-ray analysis shows that the whiskers contain Ti. Since B cannot be detected by EDAX, there is likelihood that they may be TiB or TiB_2 whiskers. The individual whiskers are 10 to 20 μm in length and about 0.5 to 1 μm in diameter. Figure 5 shows the fracture surfaces of the composition 10-10 (Ti:B:Cu = 81:9:10). Similar features are observed, including the presences of whiskers, when compared with Figure 4. It is of interest to note there are places where these whiskers are pulled out of the matrix, such as areas A and B indicated in Figure 5(a). The fracture cross section of these whiskers was never observed, indicating that their strengths are higher than the whisker-matrix interface. Figure 5(b) shows a magnified picture of whiskers.

The fracture surfaces of the Ti:B = 85:15 series compositions are shown in Figure 6. The following features are noted: (a) Compared to the compositions noted above, ductile fracture was nearly nonexistent. (b) Large particles of brittle materials were observed (*i.e.*, those which fractured in a transgranular manner). (c) All of the compositions contained whiskers. As compared to the Ti:B = 90:10 series compositions, the average diameter of the whiskers in the composition 15-0 (Ti:B:Cu = 85:15:0) was five times larger. However, in the compositions 15-10 (Ti:B:Cu = 76.5:13.5:10) and 15-20 (Ti:B:Cu = 68:12:20), the diameters decreased again to a value of approximately 2 μm.

D. *Whiskers and Combustion Temperature*

Hyman *et al.*[41] have performed extensive as-cast-binary as well as transmission electron microscopy (TEM) studies on the formation of TiB and TiB_2 in the ternary system Ti-Al-B. The crystal structures of both TiB and TiB_2 are based on the same building block and have the same needlelike morphology. The experiment shows that TiB precipitates as fine needle morphology in the binary Ti-B system and TiB_2 is only formed in the ternary Ti-B-Al system and also had needlelike morphology. It seems that there is a tendency for these materials to precipitate in needle shape. It is, therefore, difficult without extensive microscopy to determine conclusively if the whiskers are TiB or TiB_2.

Whiskers are present only in certain compositions. Andrievskii *et al.*[42] have observed similar whiskers in the Ti-B system. They experimented with various particle fractions of Ti and B and concluded that in the narrow range of combustion velocity of 0.5 to 0.8 cm/s, the TiB_2 material is formed in its crystalline structure. This can happen when, for some reasons, the high temperature is locally maintained for a longer duration and melting of TiB_2 can take place. The TiB_2 is hexagonal in structure and solidifies from the melt with a faceted interface. The combustion temperature of the various compositions are measured and shown in Table IV. The combustion temperature increases with increasing boron content and decreases with increasing copper content. Whiskers are noted to form when the combustion temperature exceeds ~950 °C. The fractographs indicate that an increase in the combustion temperature increases the diameters of whiskers.

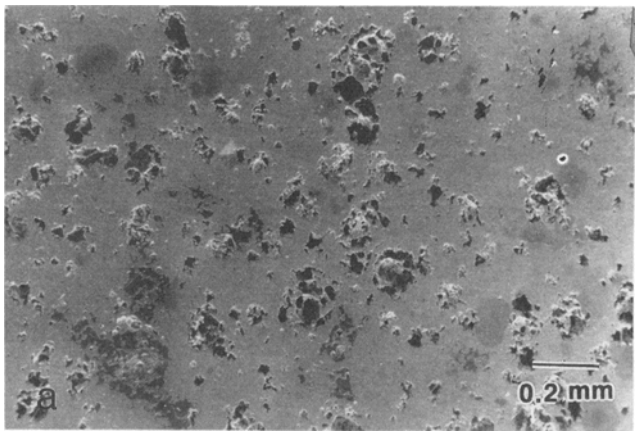

(*a*)

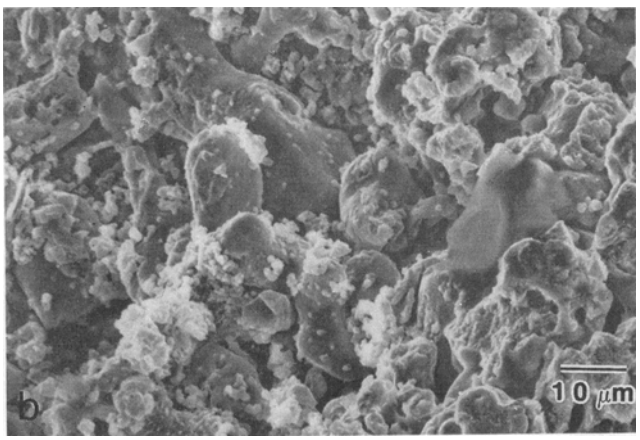

(*b*)

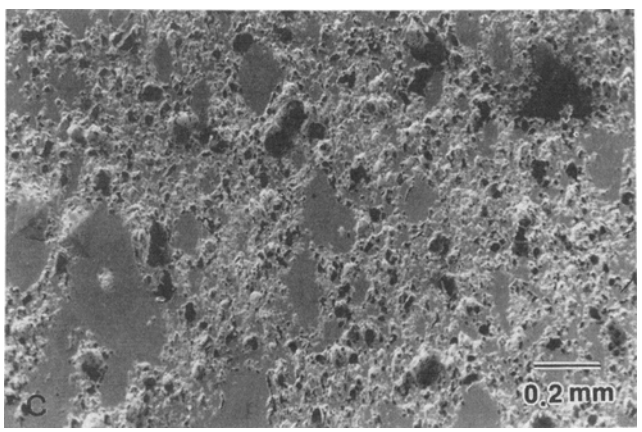

(*c*)

Fig. 2—SEM micrographs of the 10 wt pct Cu series compositions: (*a*) 10 wt pct Cu + 90 wt pct [Ti + 5 wt pct B], (*b*) 10 wt pct Cu + 90 wt pct [Ti + 10 wt pct B], and (*c*) 10 wt pct Cu + 90 wt pct [Ti + 15 wt pct B].

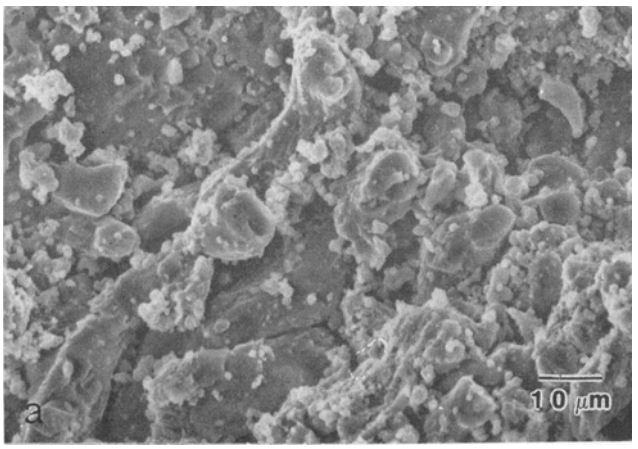

(*a*)

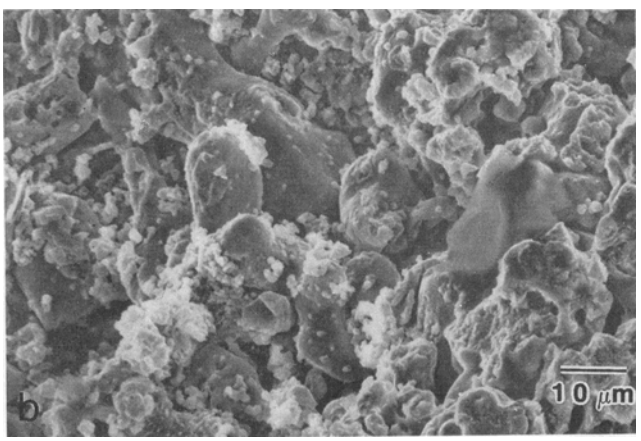

(*b*)

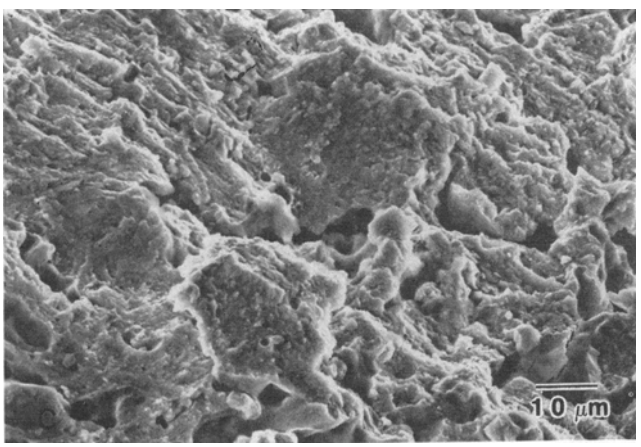

(*c*)

Fig. 3—SEM fractographs of the Ti:B = 95:5 series compositions: (*a*) 0 wt pct Cu + 100 wt pct [Ti + 5 wt pct B], (*b*) 10 wt pct Cu + 90 wt pct [Ti + 5 wt pct B], and (*c*) 20 wt pct Cu + 80 wt pct [Ti + 5 wt pct B].

E. *Fracture Toughness*

Table V shows the measured fracture toughness and hardness values of the compositions. The average fracture toughness values range between 1.6 and 8.3 MPa(m)$^{1/2}$.

As compared to the fracture toughness values reported here, conventionally sintered TiB_2 has a reported fracture toughness value of 5.00 MPa(m)$^{1/2}$.[43] The samples on which the data for sintered TiB_2 were reported[43] were made by conventional sintering; the starting powder was submicron size, produced in an arc plasma by the reaction of $TiCl_4$ and BCl_3. For achieving low-porosity

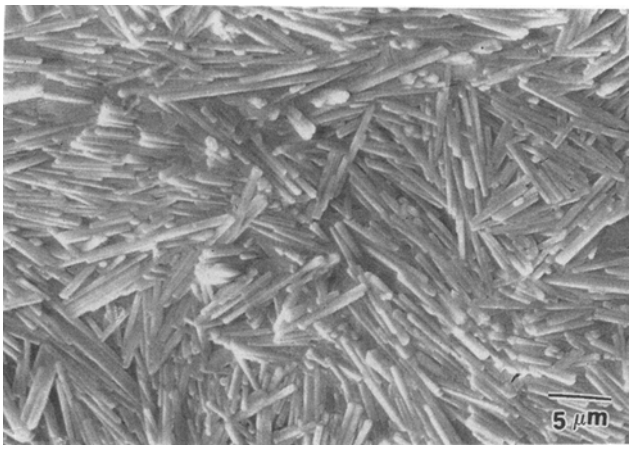

Fig. 4—Whiskers in the composition 10-0 (Ti:B:Cu = 90:10:0).

bodies, samples were sintered between 1900 °C and 2100 °C in a vacuum furnace. The value of 5.00 MPa(m)$^{1/2}$ is reported for the material sintered at 2100 °C.[43]

IV. TOUGHENING MODEL

The reasons for the high fracture toughness over that of sintered TiB_2 are explored below. In spite of the presence of pores, the fracture toughness is high. From the XRD and fractographs, it is concluded that the material contains several phases, namely:

(1) pores of various size,
(2) TiB and TiB_2 in whisker form (brittle in nature),
(3) other intermetallics based on Ti-Cu system, such as Ti_2Cu and Ti_3Cu_4. While not much is known about the Ti_3Cu_4 structure, it is well established that Ti_2Cu is isostructural with $MoSi_2$. The $MoSi_2$ has a reported fracture toughness of ~5.32 MPa(m)$^{1/2}$,[44] so it may be expected that these intermetallics are also brittle.
(4) free α-Ti, which is ductile.

It is worth examining what role each of these phases may play in influencing fracture toughness.

First, we examine the effects of porosity on the fracture toughness. It is generally believed that pores are deleterious to the mechanical properties. Vardar *et al.*[45] have studied ceramics with controlled pores subjected to tensile forces. Applying Weibill's approach, they found that the strength depends on the pore content and not on the size of the pore. They considered the decrease in the stress intensity factor and the cross-sectional area on account of the presence of pores and showed that these two factors are inadequate for the correct prediction of strength. It has been also suggested in the literature[45] that a crack associated with a pore may grow subcritically. This may partly explain why some materials show no dependence on pore size.

The relationship between the measured porosity and experimental fracture toughness values is shown in Figure 7. We note that the fracture toughness decreases as the porosity increases in the 10 and 20 wt pct Cu series compositions. The pores act as long cracks or may nucleate cracks, thus decreasing the fracture toughness.

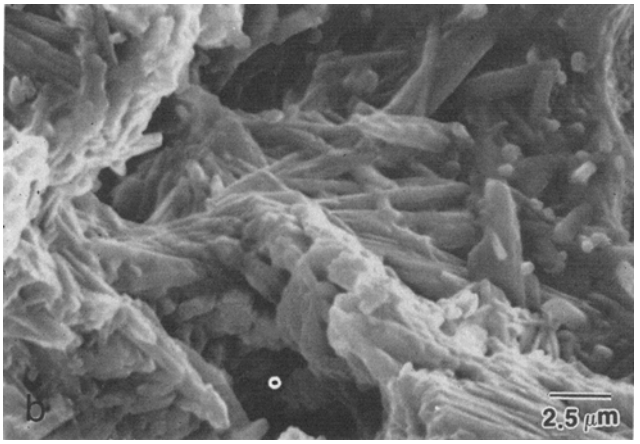

(*a*)

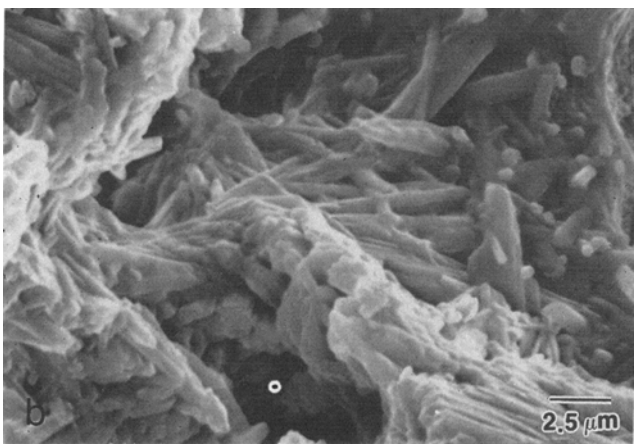

(*b*)

Fig. 5—(*a*) SEM fractograph of the composition 10-10 (Ti:B:Cu = 81:9:10) and (*b*) whiskers in the same composition (Ti:B:Cu = 81:9:10). Whisker pullout is noted in areas marked A and B in (a).

There is a possibility for whisker toughening by the TiB or TiB_2 whiskers. The phenomenon of whisker toughening is similar to ductile particle toughening. Because of the high strength of the whiskers, the area just behind the crack tip may experience a compressive stress due to intact whiskers. This reduces the crack opening displacement, and extra energy has to be spent in opening the crack tip. The modeling of the whisker toughening has been carried out by Becher *et al.*[46] The increase in fracture toughness is given by

$$\Delta K_w = \sigma_f \left(\frac{V_f r E^C G^m}{6(1 - \nu^2) E^w G^i} \right)^{1/2} \quad [3]$$

where σ_f and V_f are the fracture strength and volume fraction of whiskers, respectively, ν is Poisson's ratio, E is the Young's modulus of the composite, G is the strain energy release rate, and r is the radius of the individual whisker. The superscripts C, w, m, and i represent composite, whisker, matrix, and interface, respectively. The assumption of the model is that eventually these high-strength whiskers are fractured during crack propagation. However, the fractographs (Figures

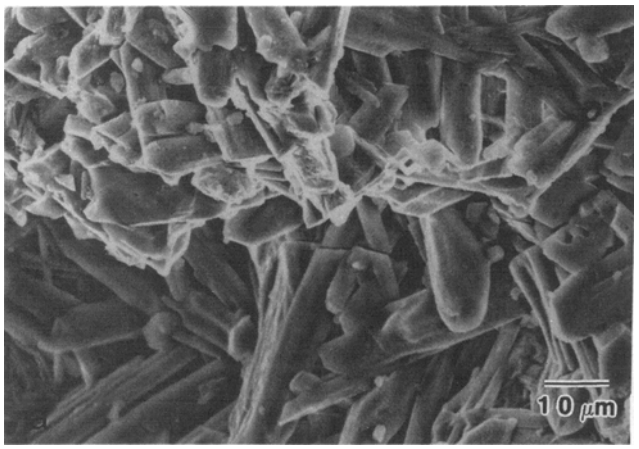

(*a*)

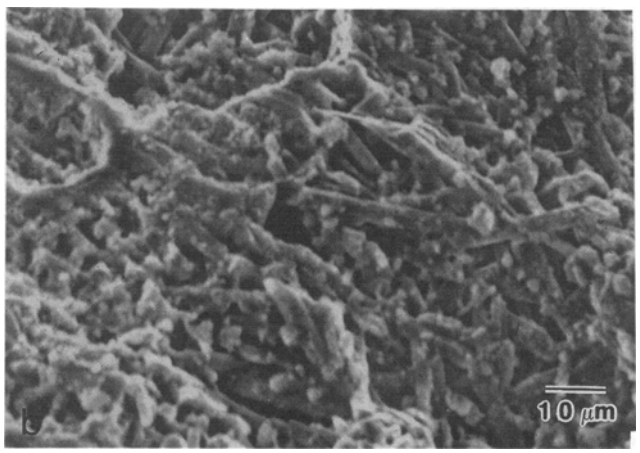

(*b*)

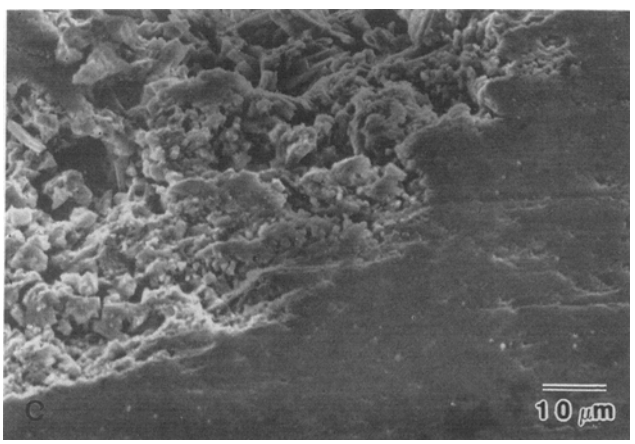

(*c*)

Fig. 6—SEM fractographs of the Ti:B = 85:15 series compositions: (*a*) 0 wt pct Cu + 100 wt pct [Ti + 15 wt pct B], (*b*) 10 wt pct Cu + 90 wt pct [Ti + 15 wt pct B], and (*c*) 20 wt pct Cu + 80 wt pct [Ti + 15 wt pct B]. The edge of the sample is seen in (c). The bottom right side of the photograph is the polished free surface. The fracture surface is the upper left part of the photograph.

Table IV. Measured Combustion Temperature for the Various Compositions*

Ti:B\Cu	0 Wt Pct Cu	10 Wt Pct Cu	20 Wt Pct Cu
Ti:B = 95:5	994 °C	756 °C	664 °C
Ti:B = 90:10	1240 °C	936 °C	898 °C
Ti:B = 85:15	1715 °C	1574 °C	1401 °C

Table V. Measured Fracture Toughness and Hardness Values for the Various Compositions

Ti:B\Cu	0 Wt Pct Cu	10 Wt Pct Cu	20 Wt Pct Cu
Toughness ($MPa(m)^{1/2}$)			
Ti:B = 95:5	3.4 ± 0.5	7.9 ± 1.1	8.3 ± 1.2
Ti:B = 90:10	4.5 ± 0.7	6.8 ± 0.9	6.6 ± 0.1
Ti:B = 85:15	1.6 ± 0.5	2.9 ± 0.4	3.8 ± 0.4
Hardness (Rockwell A Scale)			
Ti:B = 95.5	30.1 ± 4.0	37.7 ± 1.0	40.1 ± 4.2
Ti:B = 90:10	21.0 ± 5.3	41.8 ± 5.9	51.3 ± 8.3
Ti:B = 85:15	7.5 ± 0.8	11.5 ± 2.8	41.0 ± 5.6

Note: The ± values are the standard deviation 1σ values.

3 through 6) did not reveal any fractured whiskers in our experiment. Some whisker pullout has been observed (Figure 5(a)), indicating that the interface between the whisker and the matrix is weak.

The presence of other brittle phases, such as Ti_2Cu and Ti_3Cu_4, may not be beneficial also for the noted increase in fracture toughness. From the fractographs (Figures 3(b) and (c)), it is seen that they are brittle and fail in a brittle manner.

Table VI shows the volume percentages of the ductile phase and the porosity present in the system. The volume fractions of the various phases were calculated assuming the density values of Ti, TiB, and TiB_2 to be 4.50, 4.56, and 4.53 g/cm^3, respectively.[47] The density values of Ti_2Cu and Ti_3Cu_4 are not available in the literature. Crystal structures were obtained from *Pearson's Handbook*.[47] The Ti_2Cu and Ti_3Cu_4 are both tetragonal

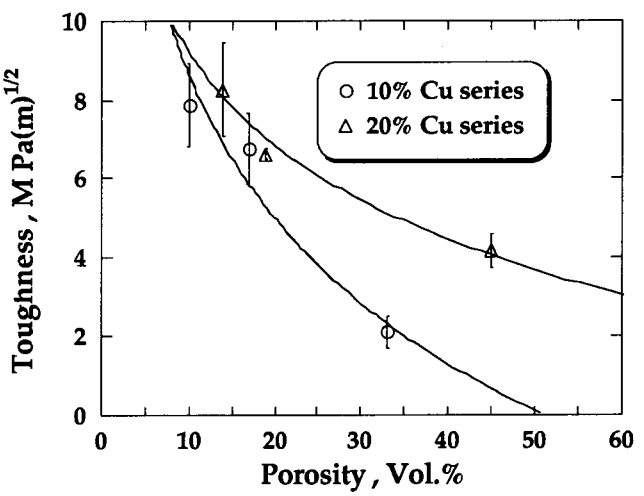

Fig. 7—Fracture toughness *vs* the porosity for the compositions with 10 and 20 wt pct Cu.

Table VI. Volume Percentages of the Ductile Phase and the Porosity in the Various Compositions

Compositions	Ti (Vol Pct)	Porosity (Vol Pct)
5-0	~40	~32
5-10	~30	~10
5-20	~22	~14
10-0	~20	~58
10-10	~23	~17
10-20	~13	~19
15-0	~ 7	~53
15-10	~ 5	~33
15-20	~ 1	~45

structures (C_{11b} and simple tetragonal, respectively). From their structures and cell parameters, the densities of Ti_2Cu and Ti_3Cu_4 are calculated to be 5.7 and 6.8 g/cm^3, respectively. Assuming the calculated values as well as the fact that all of the materials contained a certain amount of porosity, the volume percentages of the various phases may be calculated from the above density values and the relative weight ratios which are obtained from Table III. From this, the volume percentage of ductile phase was calculated.

Ductile phase toughening by Ti is now considered. From the X-ray data we note that the only ductile phase is Ti. Figure 8 shows that the experimental fracture toughness increases as the volume fraction of the ductile phase, Ti, increases in the 10 and 20 wt pct Cu series compositions. The increase in the fracture toughness value is on account of the increase in the volume fraction of the ductile phase. The increase in the ductile phases causes more energy to be spent during the crack propagation. Figure 9 shows the same relationship with compositions without Cu. The trend is the same as compositions with Cu, except for the composition 5-0. The reason for this exception is on account of the inadequate amount of B for complete combustion in this composition. Boron reacts with Ti exothermically, which produces heat to sinter or melt the rest of the Ti. In the composition 5-0, heat produced by the reaction between B and Ti is not sufficient

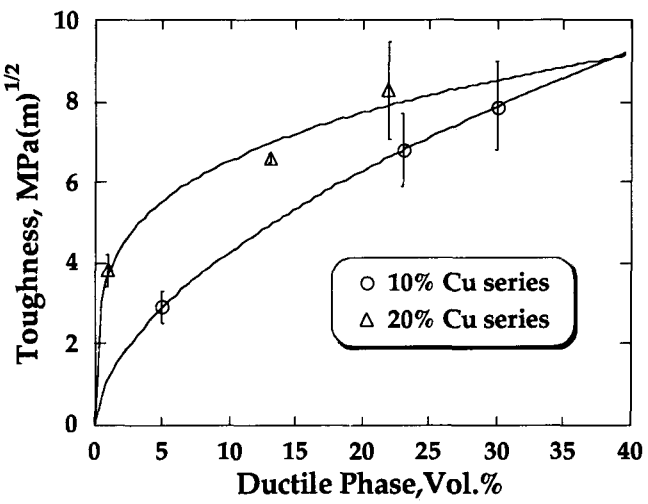

Fig. 8—Fracture toughness *vs* volume fraction of the ductile phase for the compositions with 10 and 20 wt pct Cu.

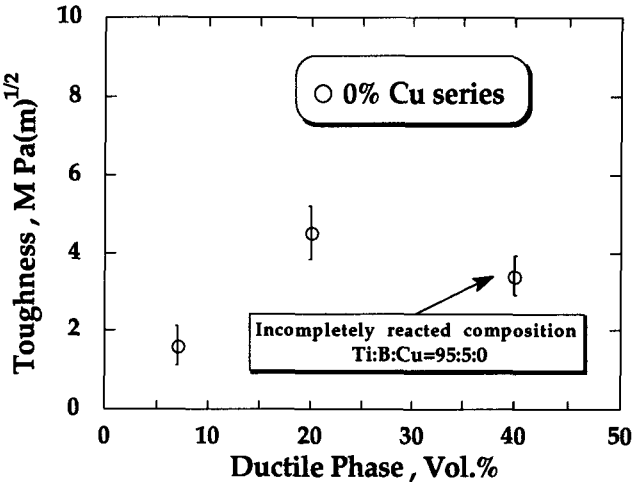

Fig. 9—Fracture toughness *vs* volume fraction of the ductile phase for the compositions without Cu.

to sinter or melt all of the Ti. The reacted product will still contain Ti (green powder), leading to lower fracture toughness in spite of the higher volume of the Ti ductile phase.

For the compositions studied in this article, the increase in fracture toughness is on account of the ductile phase and the decrease is on account of the presence of the porosity in the system. The porosity may be thought of simply modifying the base fracture toughness of the sample. We may therefore assume that the fracture toughness of the composite may be expressed as

$$K_c = K_m + \Delta K_{\text{reinforced}} - \Delta K_{\text{porosity}} + \Delta K_w \qquad [4]$$

where K_c and K_m are the fracture toughness of composite and matrix, respectively, and $\Delta K_{\text{reinforced}}$, $\Delta K_{\text{porosity}}$, and ΔK_w are the change of fracture toughness due to the reinforced ductile phase, porosity, and whisker, respectively. The term ΔK_w is taken to be zero because of the lack of whisker toughening. The value of $\Delta K_{\text{reinforced}}$ may be calculated from Ashby's model (Eq. [1]). X-ray diffraction shows that the only ductile phase is Ti. The values of the yield strength (σ_0) and Young's Modulus (E) of the ductile phase are assumed to be 98 MPa and 116 GPa,[48] respectively. The average radii of the particles (a_0) for the various compositions are measured by calculating the volume of the particles and dividing by the number of particles while making the assumption that the particles are spherical. We note that the size of the ductile phase (a_0) is linearly proportional to the volume fraction of ductile phase (V_f), as shown in Figure 10. The slopes, m's which are the ratio of a_0 to V_f, are measured to be 49.66 (μm) for 10 wt pct Cu series compositions and 45.16 (μm) for 20 wt pct Cu series compositions. After rearrangement, the Ashby's model may now be rewritten as

$$\Delta K_{\text{reinforced}} = [EC\sigma_0 m]^{1/2} V_f \qquad [5]$$

where m relates a_0 and V_f.

An interesting relationship emerges for the volume fraction of ductile phase and the porosity. This is shown in Figure 11. In the compositions containing Cu, the more the ductile metallic phase, the less the porosity, because

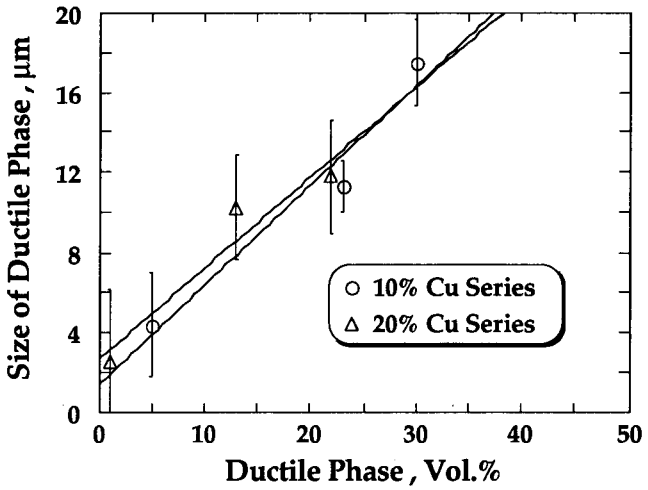

Fig. 10—Volume fraction of the ductile phase *vs* the size of the ductile phase.

the pores are filled by the molten metal formed on account of the high temperatures generated during combustion synthesis. We also note that for the compositions containing Cu if the volume fraction of the ductile phase is larger than 15 pct (region II), the porosity remains at a level of about ~15 pct in spite of increasing the volume fraction of the ductile phase. Data for the compositions without Cu are also shown in the figure. Generally speaking, the base fracture toughness of the matrix which contained pores can be described by an exponential function (Eq. [2]) in porosity, $K_m - \Delta K_{\text{porosity}} = K_{m(\text{with porosity})} = K_m \exp(-bp)$, as proposed by Kendall *et al.*,[35] Rice *et al.*[36] and Mai and Cotterell,[37] where p is porosity and b is a constant. The base fracture toughness and the matrix is assumed to be the same for the same Cu content compositions. Thus, it is assumed that the contribution to the overall fracture toughness from that part of the matrix that contains the ductile phase may be represented by Ashby's model and the part containing porosity may be expressed by Cotterell's model (exponential model) in an additive fashion. The fracture toughness of the composite may therefore be written as

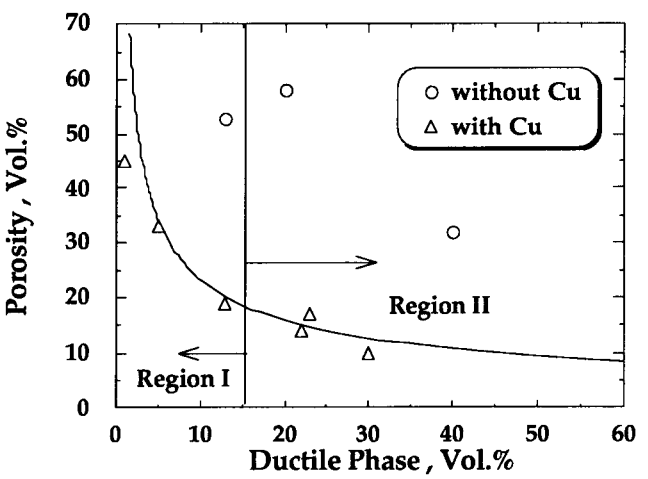

Fig. 11—Volume fraction of the ductile phase *vs* the porosity for the various compositions.

$$K_c = K_m \exp(-bp) + [EC\sigma_0 m]^{1/2} V_f \qquad [6]$$

The constants C, b, and K_m may be calculated from the experimental data for 10 and 20 wt pct Cu, respectively. The fracture toughnesses of the matrices without any porosity or ductile reinforcement are calculated to be 2.6 and 5.2 MPa(m)$^{1/2}$ for 10 and 20 wt pct Cu series compositions, respectively. The constants C and b are calculated to be 0.41 and 1.22 for the 10 wt pct Cu series compositions and 0.53 and 0.76 for 20 wt pct Cu series compositions, respectively. Comparing these values, we find that the constants for different Cu compositions are close. Although Figure 11 shows that porosity varies as a function of volume fraction of the ductile phase, the porosity term of Eq. [6], $\exp(-bp)$, only changes slightly because of the low value of b and may be considered as a constant. Therefore, K_c is proportional to the volume fraction of the ductile phase, V_f. Thus, a knowledge of K_m should be adequate for the prediction of fracture toughness of combustion-synthesized materials in the Ti-B-Cu-porosity system. Figure 12 is a plot of the dimensionless composite fracture toughness as function of the volume fraction of ductile phase divided by K_m. Note that a linear relationship with $C = 0.47$ and $b = 1$ is adequate to predict the final fracture toughness over a wide range of composition. Data for 0 wt pct Cu are also included in the figure. For the 0 wt pct, Cu, K_m was arbitrarily chosen to be 0.9 MPa(m)$^{1/2}$. The plot is linear in the range plotted, with a slope of ~16 MPa(m)$^{1/2}$ which is equal to the value of $(EC\sigma_0 m)^{1/2}$. Thus, for composites of Ti-B-Cu made by the combustion synthesis route, the increase in K_c is directly proportional to V_f and any method which enhances V_f will linearly impact on K_c.

The plot of K_c/K_m and hardness is shown in Figure 13(a). For the compositions in region I in Figure 11 where the volume fraction of ductile phase is less than 15 pct, it is seen that hardness is independent of the dimensionless fracture toughness. On the other

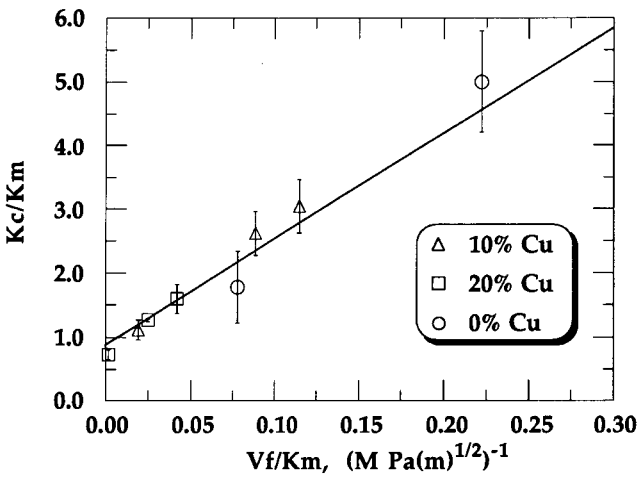

Fig. 12—Plot of the expected dimensionless fracture toughness as a function of volume fraction of the ductile phase (Ti). The experimentally determined points from 0, 10, and 20 wt pct Cu compositions are also shown in the figure. Porosity and the ductile phase are related, as shown in Fig. 11. The constants C and b of Eq. [6] are assumed to be 0.47 and 1, respectively. The value of K_m is taken to be 0.9, 2.6, and 5.2 MPa(m)$^{1/2}$ for 0, 10, and 20 wt pct Cu compositions, respectively.

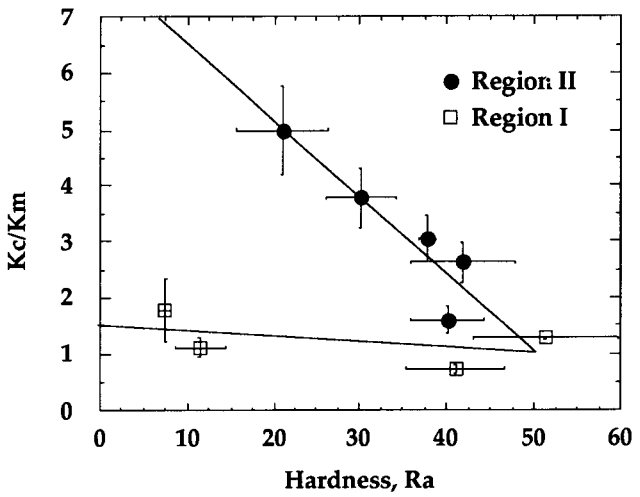

(*a*)

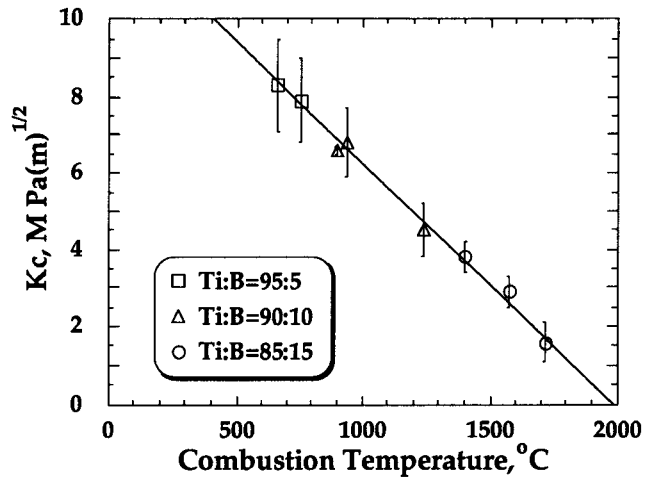

(*b*)

Fig. 13—(*a*) The plot of dimensionless fracture toughness as a function of hardness and (*b*) the plot of fracture toughness as a function of combustion temperature. The compositions in each ratio of Ti and B also contained copper as given in Table I.

hand, for the compositions in region II, hardness is inversely proportional to the dimensionless fracture toughness. Thus, a correlation exists between the hardness and toughness. Figure 13(b) shows the variation of fracture toughness and combustion temperature. An increase in combustion temperature decreases the value of K_c. The high-Ti content compositions generate less heat on combustion, have a high fraction of ductile phase, and display higher K_c values than the low-Ti content compositions. The combustion temperature is noted to be an important processing variable for determining the fracture toughness of the composites.

V. CONCLUSIONS

This article discusses the microstructural/mechanical property/processing correlation in metal/ceramic composites in the Ti-B-Cu-porosity system. The composites are fabricated by the combustion synthesis process. The following are the conclusions of the work:

The density and microstructures indicate that the composites contain porosity. With the increase in Cu, the porosity content decreases. The SEM fractographs show that there are both ductile and brittle failure regions in the composites. X-ray diffraction study shows that the only ductile phase present is free Ti. With the addition of Cu, the amount of free Ti goes down and the amount of intermetallics, such as Ti_2Cu and Ti_3Cu_4, increase. It was concluded that the ductile-phase toughening by Ti is the most important toughening mechanism for the compositions studied in this work. However, the mechanism is not fully beneficial because of the presence of porosity. The increase in fracture toughness is due to the ductile phase, and the decrease is due to the presesnce of the porosity in the system. The fracture toughness of the composites can be expressed as $K_c = K_m + \Delta K_{\text{reinforced}} - \Delta K_{\text{porosity}}$. The fracture toughness of the composite is modeled by considering the additive influence of the ductile-phase reinforcement (Ashby model) and the residual porosity (exponential model). The model is seen to predict adequately the measured values, and a linear relationship between K_c/K_m and V_f/K_m is noted in the Ti-B-Cu-porosity system. We also find a relationship between the toughness and hardness. This relationship is dependent on the volume fraction of porosity and ductile phase. The combustion temperature is noted to be an important processing variable for determining the toughness of the composites.

ACKNOWLEDGMENT

This work was supported, in part, by a grant from the Institute of Advanced Manufacturing Science, Cincinnati, OH.

REFERENCES

1. S.T. Buljan, A.E. Pasto, and H.J. Kim: *Am. Ceram. Soc. Bull.*, 1989, vol. 68, pp. 387-94.
2. J.J. Mecholsky: *Am. Ceram. Soc. Bull.*, 1989, vol. 68, pp. 367-75.
3. T.I. Mah, M.G. Mendiratta, A.P. Katz, and K.S. Mazdiyasni: *Am. Ceram. Soc. Bull.*, 1987, vol. 66, pp. 304-08.
4. J.L. Chermant and F. Osterstock: *J. Mater. Sci.*, 1976, vol. 11, pp. 1939-51.
5. M.S. Newkirk, A.W. Urquhart, H.R. Zwicker, and E. Breval: *J. Mater. Res.*, 1986, vol. 1, pp. 81-89.
6. T.B. Massalski, J.L. Murray, L.H. Bennett, and H. Baker: *Binary Alloy Phase Diagrams*, 1986, vol. 1, p. 392.
7. H.C. Yi and J.J. Moore: *J. Mater. Sci. Lett.*, 1989, vol. 8, pp. 1182-84; *J. Mater. Sci.*, 1989, vol. 24, pp. 3449-55; *J. Mater. Sci.*, 1989, vol. 24, pp. 3456-62; *J. Mater. Sci.*, 1990, vol. 25, pp. 1159-68; *J. Met.*, 1990, vol. 42 (8), pp. 31-35.
8. Z.A. Munir: *Am. Ceram. Soc. Bull.*, 1988, vol. 67, pp. 342-49.
9. S.D. Dunmead, D.W. Readey, C.E. Semler, and J.B. Holt: *J. Am. Ceram. Soc.*, 1989, vol. 72, pp. 2318-24.
10. J.B. Holt, D.D. Kingman, and G.M. Bianchini: *Mater. Sci. Eng.*, 1985, vol. 71, pp. 321-27.
11. Y. Ouabdesselam and Z.A. Munir: *J. Mater. Sci.*, 1987, vol. 22, pp. 1799-1807.
12. J.B. Holt and Z.A. Munir: *J. Mater. Sci.*, 1986, vol. 21, pp. 251-59.

13. C.T. Ho and J.A. Sekhar: in *High Temperature Ordered Intermetallic Alloys IV*, L.A. Johnson, D.P. Pope, and J.O. Stiegler, eds., MRS, Pittsburgh, PA, 1991, pp. 1057-62.
14. J. Subrahmanyan, M. Vijaykumar, and S. Ranganath: *Met. Mater. Proc.*, 1989, vol. 1, p. 105.
15. R.W. Rice, J.R. Spann, D. Lewis, and W. Coblenz: *Ceram. Eng. Sci. Proc.*, 1984, vol. 5, pp. 614-24.
16. A.J. Caputo, W.J. Lackey, and D.P. Stinton: *Ceram. Eng. Sci. Proc.*, 1985, vol. 6, pp. 694-706.
17. C.T. Forwood and A.J. Forty: *Phil. Mag.*, 1965, vol. 11, pp. 1067-82.
18. C.O. McHugh, T.J. Whalen, and M. Humenik: *J. Am. Ceram. Soc.*, 1966, vol. 49, pp. 486-91.
19. P. Hing and G.W. Groves: *J. Mater. Sci.*, 1972, vol. 7, pp. 427-34.
20. M.A. Stett and R.M. Fulrath: *J. Am. Ceram. Soc.*, 1968, vol. 51, pp. 599-600.
21. Y. Nivas and R.M. Fulrath: *J. Am. Ceram. Soc.*, 1970, vol. 53, pp. 188-91.
22. D.T. Rankin, J.J. Stiglich, D.R. Petrak, and R. Ruh: *J. Am. Ceram. Soc.*, 1971, vol. 54, pp. 277-81.
23. A.V. Virkar and D.L. Johnson: *J. Am. Ceram. Soc.*, 1977, vol. 60, pp. 514-19.
24. M.I. Mendelson and M.F. Fine: *J. Am. Ceram. Soc.*, 1974, vol. 57, pp. 154-59.
25. D.J. Green and P.S. Nicholson: in *Fracture Mechanics of Ceramics, Vol. 4*, R.C. Bradt, D.P.H. Hasselman, and F.F. Lange, eds., Plenum Publishing Corp., New York, NY, 1974, pp. 945-60.
26. A.K. Khaund and P.S. Nicholson: *J. Mater. Sci.*, 1980, vol. 15, pp. 177-87.
27. V.V. Krstic, P.S. Nicholson, and R.G. Hoagland: *J. Am. Ceram. Soc.*, 1981, vol. 64, pp. 499-504.
28. J.J. Mecholsky, T.L. Jessen, and R.H. Moore: *Ceram. Eng. Sci. Proc.*, 1985, vol. 6, pp. 657-62.
29. C.K. Elliott, G.R. Odette, G.E. Lucas, and J.W. Sheckherd: in *High-Temperature/High Performance Composites*, F.D. Lemkey, A.G. Evans, S.G. Fishman, and J.R. Strife, eds., MRS, Pittsburgh, PA, 1988, pp. 95-101.
30. J.J. Lewandowski, D. Dimiduk, W. Kerr, and M.G. Mendiratta: in *High-Temperature/High Performance Composites*, F.D. Lemkey, A.G. Evans, S.G. Fishman, and J.R. Strife, eds., MRS, Pittsburgh, PA, 1988, pp. 103-09.
31. M.F. Ashby, F.J. Blunt, and M. Bannister: *Acta Metall.*, 1989, vol. 37, pp. 1847-57.
32. H.C. Cao, B.J. Dalgleish, H.E. Deve, C. Elliott, A.G. Evans, R. Mehrabian, and G.R. Odette: *Acta Metall.*, 1989, vol. 37, pp. 2969-77.
33. A.G. Evans, A.H. Heuer, and D.L. Porter: in *Fracture 1977*, D.M.R. Taplin, ed., University of Waterloo Press, Waterloo, Canada, 1977, vol. I, pp. 529-53.
34. A.G. Evans and R.M. McMeeking: *Acta Metall.*, 1986, vol. 34, pp. 2435-41.
35. K. Kendall, A.J. Howard, and J.D. Birchall: *Phil. Trans. R. Soc. London*, 1983, vol. A310, p. 139.
36. R.W. Rice, S.W. Freiman, R.C. Pohanka, J.J. Melcholsky, and C.C. Wu: in *Fracture Mechanics of Ceramics, Vol. 4*, R.C. Bradt, D.P.H. Hasselman, and F.F. Lange, eds., Plenum Publishing Corp., New York, NY, 1974, pp. 849-76.
37. Y.W. Mai and B. Cotterell: *Cement Concrete Res.*, 1985, vol. 15, pp. 995-1002.
38. *Annual Book of ASTM Standards*, ASTM, Philadelphia, PA, 1989, vol. 15.02, pp. 109-110.
39. G.K. Bansal and W.H. Duckworth: in *Fracture Mechanics Applied to Brittle Materials*, S.W. Freiman, ed., ASTM, Philadelphia, PA, 1978, pp. 38-46.
40. I. Barin, O. Knacke, and O. Kubaschewski: *Thermochemical Properties of Inorganic Substances*, Springer-Verlag, New York, NY, 1973, pp. 791-92.
41. M.E. Hyman, C. McCullough, J.J. Valencia, C.G. Levi, and R. Mehrabian: *Metall. Trans. A.*, 1989, vol. 20A, pp. 1847-59.
42. R.A. Andrievskii, A.T. Pak, and I.F. Baiman: *Sov. Powder Metall. Metal Ceram.*, 1989, vol. 28, pp. 669-71.
43. H.R. Baumgartner and R.A. Steiger: *J. Am. Ceram. Soc.*, 1984, vol. 67, pp. 207-12.
44. F.D. Gac and J.J. Petrovic: *J. Am. Ceram. Soc.*, 1985, vol. 68, pp. C.200-01.
45. O. Vardar, I. Finnie, D.R. Biswas, and R.M. Fulrath: *Int. J. Fracture*, 1977, vol. 13, pp. 215-23.
46. P.F. Becher, C.H. Hsueh, P. Angelini, and T.N. Tiegs: *J. Am. Ceram. Soc.*, 1988, vol. 71, pp. 1050-61.
47. P. Villars and L.D. Calvert: *Pearson's Handbook of Crystallographic Data for Intermetallic Phases, Vol.* 2, ASM, Metals Park, OH, 1985, pp. 2036-37.
48. *Guide to Materials Engineering Data and Information*, ASM INTERNATIONAL, Metals Park, OH, 1986, p. 2.10.